Available at
http://pvamu.edu/aam
Appl. Appl. Math.
ISSN: 1932-9466

Applications and Applied Mathematics:
An International Journal
(AAM)

Vol. 11, Issue 2 (December 2016), pp. 663 -679

Impact of Permeable Lining of the Wall on the Peristaltic Flow of Herschel Bulkley Fluid

G. C. Sankad[1] and Asha Patil

Research Centre
Department of Mathematics
B.L.D.E.A.'s V. P. Dr. P. G. Halakatti College of Engineering and Technology
Vijayapur – 586103
Karnataka, India
(Affiliated to Visvesvaraya Technological University, Belagavi)
[1]email: math.gurunath@bldeacet.ac.in

Received: April 11, 2016; Accepted: August 20, 2016

Abstract

The peristaltic motion is modeled for the Herschel Bulkley fluid, considered to flow in a non-uniform inclined channel. The channel wall is supposed to be lined with a non-erodible porous material. The flow is considered to be moving in a wave frame of reference moving with same velocity as of the sinusoidal wave. Low Reynolds number and long wave length assumptions are made to solve the model. Analytical solution is obtained for the pressure difference and also for the frictional force. Graphs are plotted, using Mathematica software, for both the results of pressure difference and frictional force against time average velocity. We observe that increasing the porous thickening, increases the pressure difference while, it decreases the frictional force. It is seen that the behavior of the pressure difference is opposite to the behavior of the frictional force for all the parameters considered.

Keywords: Herschel Bulkley fluid; Non-uniform channel; Porous; Inclined; Pressure difference; Frictional force

MSC 2010 No.: 76Z05, 76A05, 35C05

Nomenclature:

a	half width of the channel at the inlet.	V	transverse velocity in the laboratory frame.
a_0	half width of the channel.	x	axial coordinate in the wave frame.
d	amplitude of the wave.	X	axial coordinate in the laboratory frame.
c	wave speed.	y	transverse coordinate in the wave frame.
Da	Darcy number.	Y	transverse coordinates in the laboratory frame.
F	frictional force at the wall.	y_0	plug flow width.
H	expression defined by (1).	α	slip parameter.
N	index parameter.	ϵ	porous thickening of the wall.
p	pressure.	θ	angle of inclination.
P	expression defined in (9).	λ	wave length.
q	volume flux.	τ	yield stress.
Q	instantaneous volume flow rate.	τ_{yx}	shear stress.
$\bar{Q}$	time average volume flow.	ψ	stream function.
T	time.	ΔP	pressure difference.
u	axial velocity in the wave frame.		
U	axial velocity in the laboratory frame.		

1. Introduction

Peristalsis' the mechanism of fluid transport through the elastic pipe by means of a sinusoidal wave, is an important action enabling many biological and mechanical processes viz., the transport of urine through ureter, chyme in the esophagus, ovum in the female fallopian tube, blood transport in the heart lung machine and many more.

Many authors (Misra and Rao (2003), Abd El Hakeem et al. (2002), Ebaid (2008)) have considered Newtonian fluid model for their study. Tang and Fung (1975) and many authors have considered blood and other biofluids to behave like a Newtonian fluid for physiological peristalsis. Although the Newtonian approach of blood gives satisfactory results for the ureter mechanism, it fails to do so in small blood vessels and intestine.

Studies suggest that the behavior of blood is more likely to be non-Newtonian (Majhi and Nair (1996)). Through the investigations it is accepted that blood in small arteries and fluids in the lymphatic vessels and in intestine, urine under certain pathological conditions, and so on, behave like non-Newtonian fluids. Also, although the solution of non-Newtonian fluids is complex due to the appearance of the non-linear term, the flow of blood in human body, alloys and metals in industries, mercury amalgams and lubrication with heavy oils and greases in machines, are few examples of flow of non-Newtonian fluids that show us how important is the study of non-Newtonian fluids.

The first quantitative approach on the peristaltic flow of non-Newtonian fluids was made by Raju and Devanathan (1972). Various authors (Mekheimer (2002); Sobh (2008)) have put forth their investigations on the peristaltic flow, considering uniform and non-uniform channels with different fluids and their corresponding parameters. Recently, applying the homotopy perturbation method, Ali et al. (2016) have investigated the peristaltic flow of hyperbolic tangent fluid through a three dimensional non-uniform channel with flexible walls

and concluded that the velocity is maximum at the center of the channel but is minimum at the walls.

Applying Darcy's law many researchers have carried on their study through porous medium, as submitted by Scheidegger (1974). Mishra and Ghosh (1997) considered the small blood vessels in lungs to be porous channels and analyzed the pressure and velocity distribution numerically. Shahawey et al. (2006) inspected the peristaltic motion through a porous symmetric channel. The wall effects of the peristaltic flow of a hyperbolic tangential fluid are studied by Nagachandrakala et al. (2013), through a porous non-uniform channel. Ramesh and Devakar (2015) have analyzed the peristaltic motion considering the MHD Williamson fluid in an inclined asymmetric channel under heat transfer in a porous medium. Several authors (Ellahi (2014), Ali et al. (2015)) have studied the application of peristaltic flow, in porous media and in non-uniform channel. Bhatti et al. (2016) have studied the peristaltic flow of blood modeled as a Jeffery fluid, through a porous medium, analyzing the simultaneous effect of slip and MHD. This study reveals that the increase in slip and the porosity parameter decreases the pressure rise whereas increase in the Hartmann number increases the pressure rise.

The study of peristaltic flow in a deformable inclined tube was done by Abd El Hakeem et al. (2007), under the wall slip conditions. Ramanakumari and Radhakrishnamacharya (2011) discussed the slip effects with wall conditions on the peristaltic flow in an inclined channel. Riahi and Roy (2011) studied the flow in a tube and in an annulus respectively, representing the flow of chyme in the small intestine, in the absence and presence of a cylindrical endoscope. Considering the micro polar fluid, Krishna Kumari et al. (2013) have analyzed the peristaltic flow under the magnetic effect in an inclined channel. Smita and Anamol Kumar (2013) examined the blood flow through arteries under peristalsis. Rathod and Sridhar (2015) analyzed the peristaltic motion in an inclined channel and concluded that, with increase in the angle of inclination, pressure rise and the frictional force both increase.

Yet another non-Newtonian fluid is the Herschel Bulkley fluid whose constitutive equation can be reduced to study the Newtonian behavior also. Peristaltic motion of Herschel Bulkley fluid through a channel with flexible wall is studied by Vajravelu et al. (2005). Medhavi's (2008) study exposed that, the association between the pressure and the flow rates are linear in Bingham and Newtonian fluid models and are non-linear in Herschel-Bulkley and power-law models. Sankad et al. (2014) investigated the effects of wall on the peristaltic motion of a Herschel-Bulkley fluid in a non-uniform channel. Hummady and Abdulhadi (2014) studied the effects of slip and heat transfer on the peristaltic motion under MHD considering the flow of non-Newtonian fluid in a porous medium. Considering the Herschel Bulkley fluid, Akbar and Butt (2015) have examined the heat transfer effect on the peristaltic transport through a non-uniform channel.

The Herschel Bulkley fluid describes the behavior of shear thinning and shear thickening fluids which have applications in Biomedical engineering. The study of Herschel Bulkley fluid is more emphasized since, blood behaves similar to Herschel Bulkley fluid rather than power law and Bingham fluids, thus making it is applicable in the analysis of blood and other physiological fluid flows stimulated by peristalsis. Herschel Bulkley fluid model is considered to be a better model for flow of blood in arterioles and therefore it might also help in the clinical procedure of blood transportation using the heart lung machine and roller pumps. In the microcirculatory system, the Reynolds number and the ratio of half width of

the channel to the wavelength are small and lubrication theory can be applied for the theoretical analysis

It is observed that the gastro intestinal tract is enclosed by many innervated smooth muscle layers whose contraction mix the contents and helps in the controlled movement of food. These layers consist of many folds having pores through its tight junctions which help in the absorption of nutrients and water. It is also noticed that several ducts in physiological structure are inclined to the axis.

Interestingly, apart from numerous theoretical studies, many experimental investigations (Hung and Brown (1976), Brown and Hung (1977)) are carried out in the moving and fixed frame, on the peristaltic fluid flows. The studies have realized that the fluid within the bolus moves with a net advance velocity equal to the wave speed and thus giving rise to steady flow.

Through this motivation, the Herschel Bulkley fluid model is considered for our study of peristaltic flow through a non-uniform inclined conduit. The walls of the channel are lined with porous material. Lubrication approach is applied to analyze the distribution of velocity of blood and pumping characteristics.

2. Mathematical Formulation

Consider the Herschel–Bulkley fluid moving in a channel of half width 'a_0' lined with non-erodible porous material. The flexible wall of the channel is subjected to a progressive peristaltic wave with amplitude *'d'*, wave length 'λ' and wave speed '*c'*. The channel under consideration is non-uniform and inclined at an angle 'θ'. The discussion is considered for only the half width of the channel. In the plug flow region i.e. in the region between $y = 0$ and $y = y_0$ we have $|\tau_{xy} \leq \tau_0|$ and for the region between $y = y_0$ and $y = H$, $|\tau_{xy}| \geq \tau_0$. The deformation of the wall is given by,

$$Y = H(X,t) = a_0 + d\, sin\, \frac{2\pi}{\lambda}(X - ct). \tag{1}$$

Here, $a_0 = a + bx$, where a represents the half width of the channel at the inlet. Also, assuming the length of the channel to be an integral multiple of the wavelength λ and the pressure difference to be constant across the ends of the channel, there is steady flow in the wave frame (x, y), moving with the velocity 'c' away from the laboratory frame (X, Y). The flow is unsteady in the laboratory frame (X, Y), however in the co-ordinate system moving with the propagation velocity c, in the wave frame (x, y) the boundary shape is stationary (Shapiro et al. (1969)).

The relation between these two wave frames is given by

$$x = X - ct\ ; \quad y = Y\ ; \quad u(x,y) = U(X\text{-}ct, Y)\text{-}c\ ;$$
$$v(x,y) = V(X\text{-}ct, Y)\ ;\ p(x) = p(X,t)\,.$$

where *U* and *V* are components of velocity in the laboratory frame and *u*, *v* are components of velocity in the wave frame. As proved experimentally, the Reynolds number of the flow is very small in many physiological situations. We assume inertia free flow with infinite wavelength. To formulate the basic equations and the boundary conditions to be dimensionless, the following quantities are used:

$$x' = \frac{x}{\lambda};\quad \mathrm{y}' = \frac{\mathrm{y}}{\mathrm{d}};\quad \mathrm{h}' = \frac{\mathrm{h}}{\mathrm{a}};\quad t' = \frac{ct}{\lambda};\varepsilon' = \frac{\varepsilon}{a};$$
$$\psi' = \frac{\psi}{ac};\quad q' = \frac{q}{ac};\quad u' = \frac{u}{c};\quad \varphi' = \frac{b}{a};\quad Da = \frac{k}{a^2};$$
$$b' = \frac{b\lambda}{a};\quad d' = \frac{d}{a};\quad \tau_0' = \frac{\tau_0}{\mu c^n/a};\quad \mathrm{F}' = \frac{\mathrm{fa}}{\mu\lambda \mathrm{c}}.$$

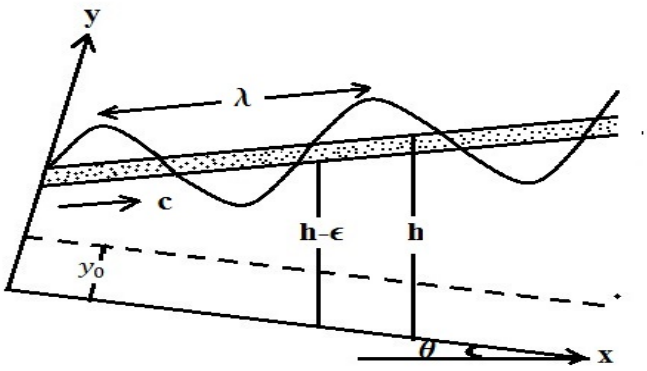

Figure A. Geometry of the flow.

Under the presumptions of long wavelength and low Reynolds number, the governing equations of motion after declining the primes are as follows:

$$\frac{\partial}{\partial y}(\tau_{yx}) = -\frac{\partial p}{\partial x} + \eta\, sin\theta, \tag{2}$$

where

$$\tau_{yx} = \left(-\frac{\partial u}{\partial y}\right)^n + \tau_0\,, \tag{3}$$

and the boundary conditions are

$$\psi = 0 \;\; at \;\; y = 0, \tag{4}$$

$$\psi_{yy} = 0 \;\; at \;\; y = 0, \tag{5}$$

$$\tau_{yx} = 0 \;\; at \;\; y = 0\,, \tag{6}$$

$$u = -\frac{\sqrt{Da}}{\alpha}\frac{\partial u}{\partial y} - 1, \;\; at \;\; y = h(x) - \epsilon, \tag{7}$$

where

$$h(x) = 1 + bx + \; d\; sin\; 2\pi x.$$

3. Solution of the problem

Solving Equations (2) and (3) along with $u = \frac{\partial \psi}{\partial y}$, $v = -\frac{\partial \psi}{\partial x}$ and the boundary conditions (4) - (7), we get the velocity field as,

$$u = P^m \left[\frac{1}{m+1}\{(h-\epsilon-y_o)^{m+1} - (y-y_o)^{m+1}\} + \frac{\sqrt{Da}}{\alpha}(h-\epsilon-y_o)^m\right] - 1\,, \qquad (8)$$

where

$$P = -\frac{\partial p}{\partial x} + \eta\, sin\theta \text{ and } m = \frac{1}{n}. \qquad (9)$$

In the plug flow region the upper limit $y_0 = \frac{\tau_0}{p}$, is obtained taking the boundary condition $\psi_{yy} = 0 \;\; at \;\; y = y_0$.

The condition $\tau_{xy} = \tau_{h-\epsilon}$ at $y = h - \epsilon$, is applied to get $P = \frac{\tau_{h-\epsilon}}{h-\epsilon}$. Therefore,

$$\frac{y_0}{h-\epsilon} = \frac{\tau_o}{\tau_{h-\epsilon}} = \tau\,;\; 0 < \tau < 1.$$

To obtain the velocity in the plug flow region, we consider $y = y_o$ in (8) and get,

$$u_p = P^m (h-\epsilon-y_o)^m \left(\frac{h-\epsilon-y_o}{1+m} + \frac{\sqrt{Da}}{\propto}\right) - 1. \qquad (10)$$

Equations (8) and (10) are integrated along with the conditions $\psi_p = 0$ at $y = 0$ and $\psi = \psi_p$ at $y = y_o$ obtain the stream functions as

$$\psi = P^m \left[\frac{1}{m+1}\left\{(h-\epsilon-y_o)^{m+1} y - \frac{(y-y_o)^{m+2}}{m+2}\right\} + \frac{\sqrt{Da}}{\alpha}(h-\epsilon-y_0)^m\, y\right] - y, \qquad (11)$$

$$\psi_p = \int u_p dy = P^m (h-\epsilon-y_0)^m \left(\frac{h-\epsilon-y_0}{m+1} - \frac{\sqrt{Da}}{\alpha}\right) y - y\,. \qquad (12)$$

The volume flux across each cross section, denoted by 'q' is given by

$$q = \int_0^{y_0} u_p dy + \int_{y_0}^{h-\epsilon} u\, dy.$$

$$q = P^m \left[\frac{(h-\epsilon-y_0)^{m+1}}{m+1}\left\{h-\epsilon - \frac{(h-\epsilon-y_0)}{m+2}\right\} + (h-\epsilon-y_0)^m \frac{\sqrt{Da}}{\alpha}(h-\epsilon)\right] - (h-\epsilon). \qquad (13)$$

From Equations (9) and (13) we get,

$$\frac{\partial p}{\partial x} = -P + \eta \sin\theta$$

$$= \left[\frac{-(q+h-\varepsilon)(m+1)(m+2)\alpha}{(h-\varepsilon)^{m+1}(1-\tau)^m \left\{ \alpha(h-\varepsilon)(1-\tau)\{(m+2)-(1-\tau)\} + \sqrt{Da}(m+1)(m+2) \right\}} \right]^{\frac{1}{m}} + \eta \sin\theta . \quad (14)$$

The instantaneous volume flow rate $Q(X,t)$, between the central line and the wall, in the laboratory frame is

$$Q(X,t) = \int_0^H U(X,Y,t)\, dY. \quad (15)$$

Averaging Equation (15) on one period, yields the time-averaged volume flow rate $\bar{Q}$ as,

$$\bar{Q} = \frac{1}{T}\int_0^T Q dt = q + 1. \quad (16)$$

Integrating Equation (14) over one wavelength, the pressure difference over a cycle of the wave is given as

$$\Delta P = \int_0^1 \frac{\partial p}{\partial x}\, dx = \int_0^1 (-P + \eta\, sin\theta)\, dx. \quad (17)$$

The frictional force *F*, at the wall over one wavelength is

$$F = \int_0^1 h\left(-\frac{\partial p}{\partial x}\right) dx = \int_0^1 h(P - \eta\, sin\,\theta)\, dx\,. \quad (18)$$

4. Results and Discussion

Graphs are plotted for Equation 17, using Mathematica software, for the pressure difference ΔP against time-averaged volume flow rate $\bar{Q}$.

As the Darcy number increases, ΔP decreases up to $\bar{Q} = 0.3$ and opposite behavior is observed for $\bar{Q} > 0.5$. For, $0.3 < \bar{Q} < 0.5$, the variation of $\bar{Q}$ hardly has any effect on ΔP for a divergent channel $(b = 0.1)$ as shown in Figure 1. Figure 2 shows a similar effect in the convergent channel $(b = -0.1)$ except for the region where we observe no effect is $0.5 < \bar{Q} < 0.7$.

The opposite behavior is seen for variation of the yield stressτ. Figure 3 depicts that the curves intersect at $\bar{Q} = 0.4$ and it is seen that to the left, ΔP increases with τ whereas, to the right of this point of intersection, ΔP decreases with increase in τ in a divergent channel. Again, a similar effect is observed for a convergent channel, but for the point of convergence being 0.5 as observed from Figure 4.

Figures 5 and 6 depict the effect of ϵ. As the porous thickening ϵ increases, pumping increases and the effect of the porous thickening on the wall is negligible on ΔP once the pumping curves intersect. The pumping curves intersect at $\bar{Q} = 0.5$ in a divergent channel and at $\bar{Q} = 0.7$ in a convergent channel.

We also observe from Figure 7 and Figure 8 that the pumping increases, with increase in the angle of inclination θ in the divergent channel as well in the convergent channels, respectively. We notice that the effect is less in the convergent channel compared to a divergent channel.

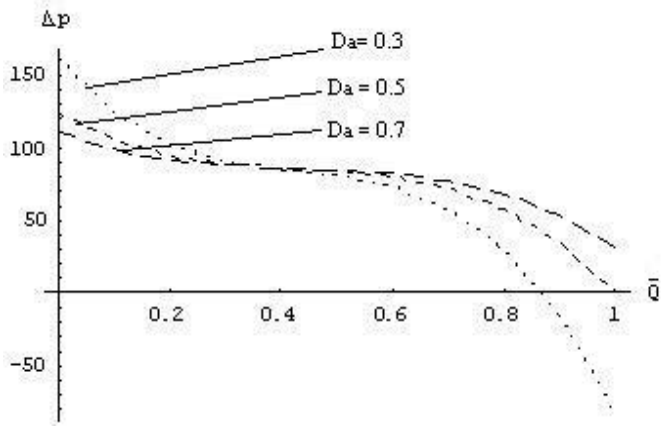

Figure 1. $n = 3$; $= 0.3$; $= 0.3$; $= 0.1$; $= 0.1$; $= /3$. Illustration of pressure difference with the volume flow rate for various values of Darcy number in a divergent channel.

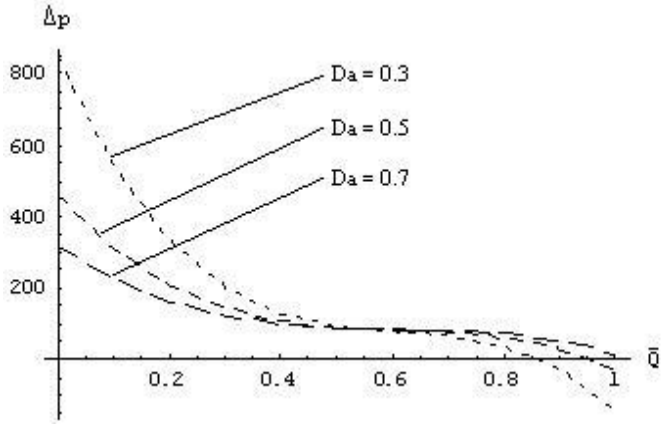

Figure 2. $n = 3$; $= 0.3$; $= 0.3$; $= 0.1$; $= 0.1$; $= /3$. Illustration of pressure difference with the volume flow rate for various values of Darcy number in a convergent channel.

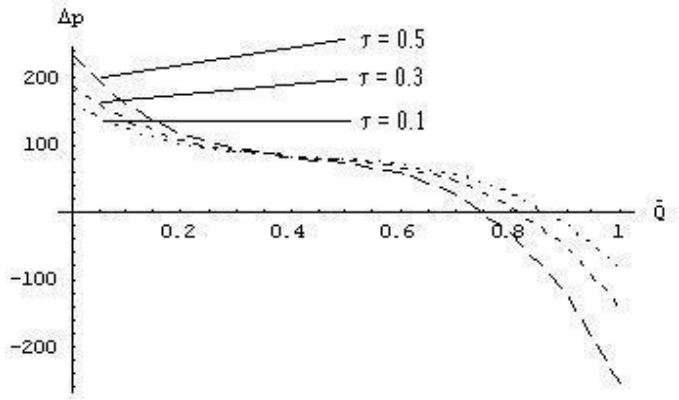

Figure 3. $n = 3$; $= 0.3$; $= 0.3$; $Da = 0.3$; $= 0.1$; $= /3$. Illustration of pressure difference with the volume flow rate for various values of yield stress in a divergent channel.

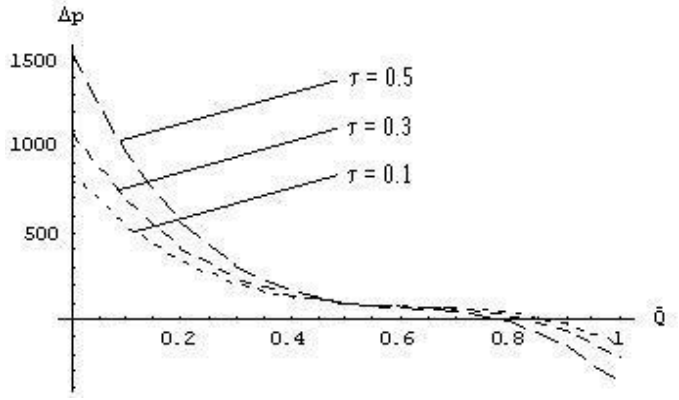

Figure 4. $n = 3$; $= 0.3$; $= 0.3$; $Da = 0.3$; $= 0.1$; $= /3$. Illustration of pressure difference with the volume flow rate for different values of yield stress in a convergent channel.

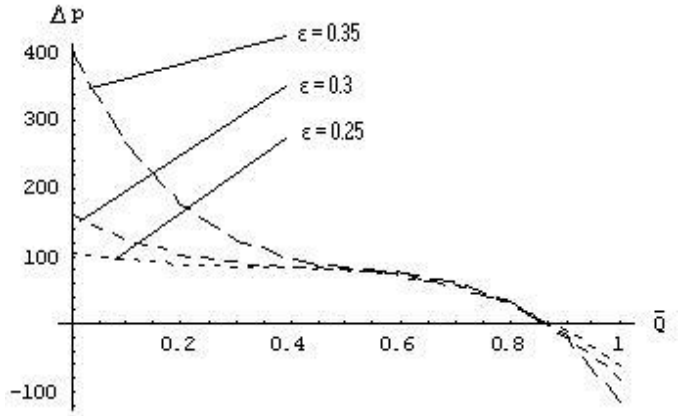

Figure 5. $n=3$; $=0.3$; $Da=0.3$; $=0.1$; $=0.1$; $= /3$. Illustration of pressure difference with the volume flow rate for various values of porous thickening of the wall in a divergent channel.

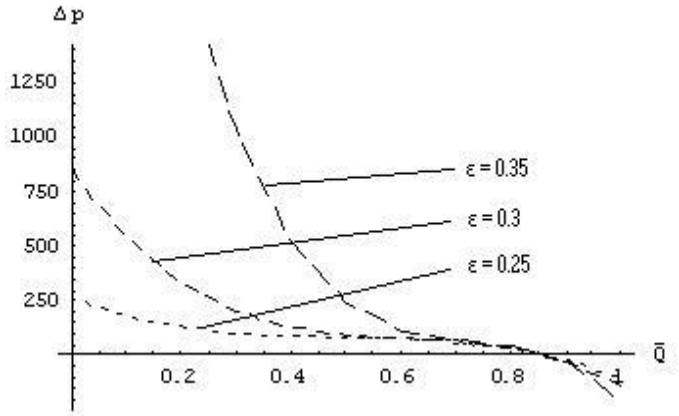

Figure 6. *n=3; =0.3; Da=0.3; =0.1; =0.1; = /3.* Illustration of pressure difference with the volume flow rate for various values of porous thickening of the wall in a convergent channel.

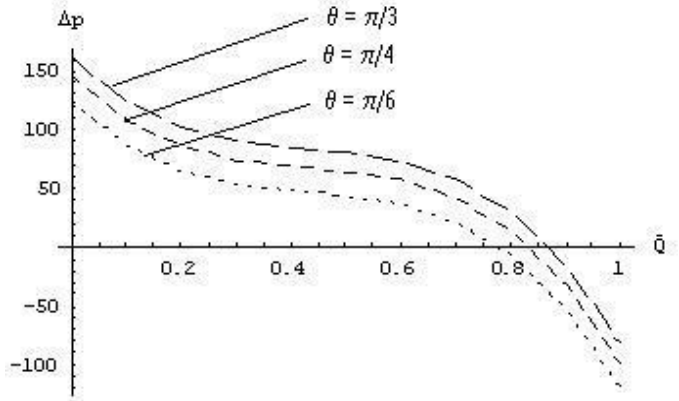

Figure 7. *n=3; =0.3; Da =0.3; =0.3; =0.1; =0.1*. Illustration of pressure difference with the volume flow rate for various values of inclination of the channel in a divergent channel.

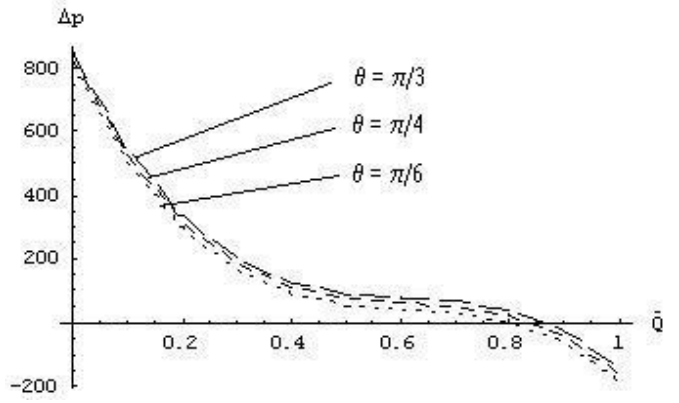

Figure 8. *n=3; =0.3; Da =0.3; =0.3; =0.1; =0.1.* Illustration of pressure difference with the volume flow rate for various values of inclination of the channel in a convergent channel.

Using Equation (18), graphs of frictional force F against time-averaged volume flow rate $\bar{Q}$ are plotted.

Figure 9 shows that the increase in Darcy number increases the frictional force up to $\bar{Q} = 0.4$ and further it is seen that the frictional force decreases with increase in the Darcy number in the convergent channel. The same effect of Darcy number is observed in the divergent channel also as plotted in Figure 10; i.e. the frictional force increases with Darcy number up to $\bar{Q} = 0.5$ and then it decreases with Darcy number.

The graphs for the variation of τ are shown in Figure 11 and Figure 12. We observe that as τ increases, the frictional force decrease up to $\bar{Q} = 0.3$ in a divergent channel and up to $\bar{Q} = 0.5$ in a convergent channel and then onwards it is seen that increase in τ increases the frictional force *F*.

As the porous thickening ϵ increases, the frictional force *F* decreases up to $\bar{Q} = 0.5$. For $0.5 < \bar{Q} < 0.8$, variation of ϵ has no effect on the increase in *F*, but further increase in ϵ increases the frictional force as observed from Figure 13. A similar effect is observed from Figure 14 in a convergent channel, except for the null effect region being $0.7 < \bar{Q} < 0.9$.
With increase in the inclination θ, we observe a drop in the frictional force for both convergent and divergent channels as plotted in Figure 15 and Figure 16, respectively. What we observe here is that variation of angle of inclination has less effect on a convergent channel compared to the divergent channel.

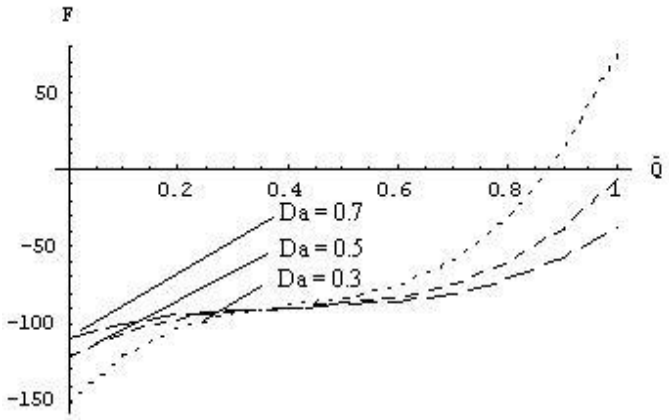

Figure 9. *n=3; =0.3; =0.3; =0.1; =0.1; = /3.* Illustration of frictional force with the volume flow rate for various values of Darcy number in a divergent channel.

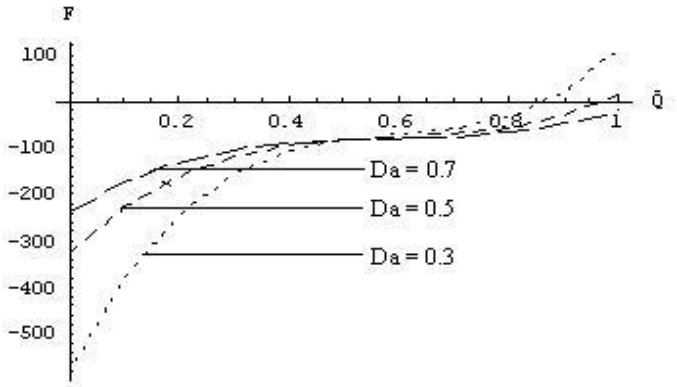

Figure 10. *n=3; =0.3; =0.3; =0.1; =0.1; = /3.* Illustration of frictional force with the volume flow rate for various values of Darcy number in a convergent channel.

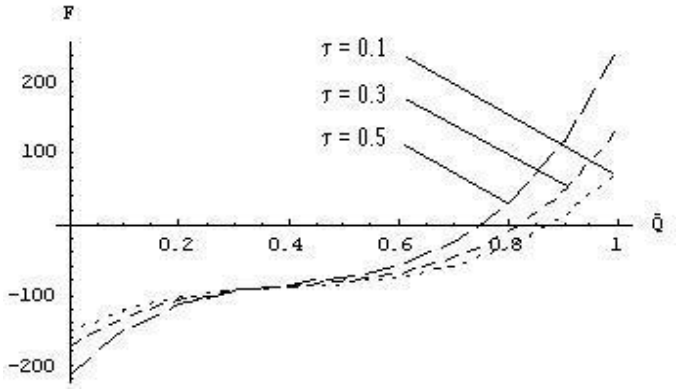

Figure 11. *n=3; =0.3; =0.3; Da =0.3; =0.1; = /3*. Illustration of frictional force with the volume flow rate for various values of yield stress in a divergent channel.

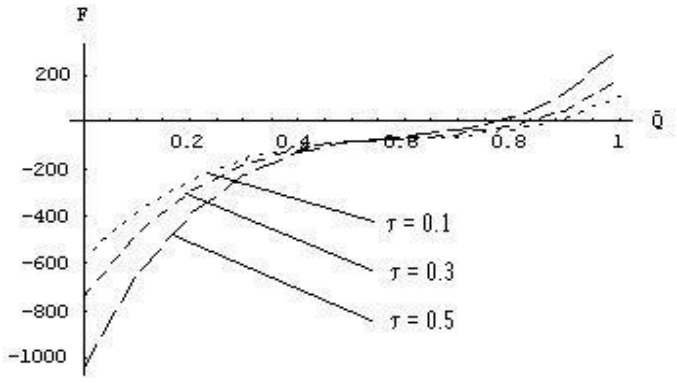

Figure 12. *n=3; =0.3; =0.3; Da =0.3; =0.1; = /3;* Illustration of frictional force with the volume flow rate for various values of yield stress in a convergent channel.

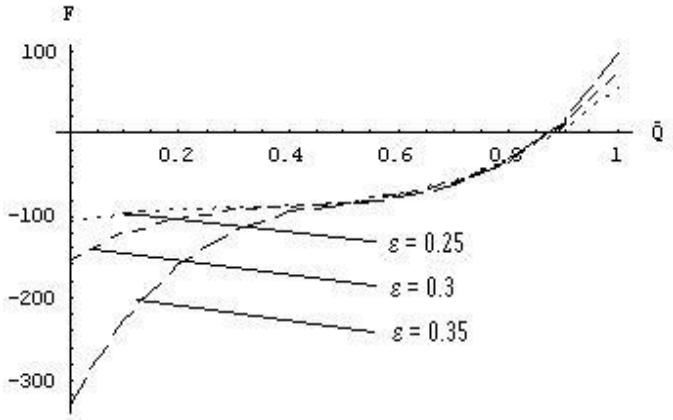

Figure 13. *n=3; =0.3; Da =0.3; =0.1; =0.1; = /3.* Illustration of frictional force with the volume flow rate for various values of porous thickening of the wall in a divergent channel.

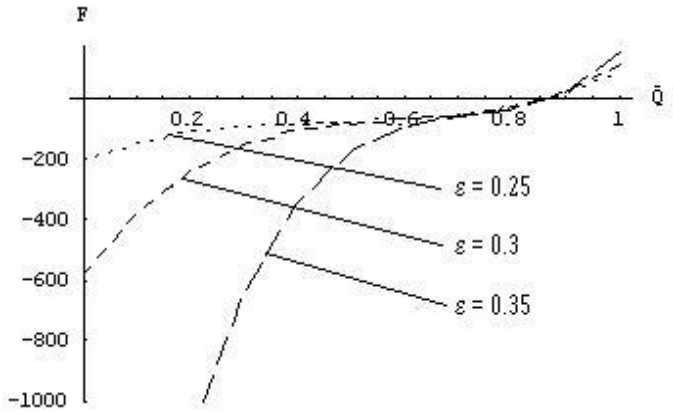

Figure 14. *n=3; =0.3; Da =0.3; =0.1; =0.1; = /3.* Illustration of frictional force with the volume flow rate for various values of porous thickening of the wall in a convergent channel.

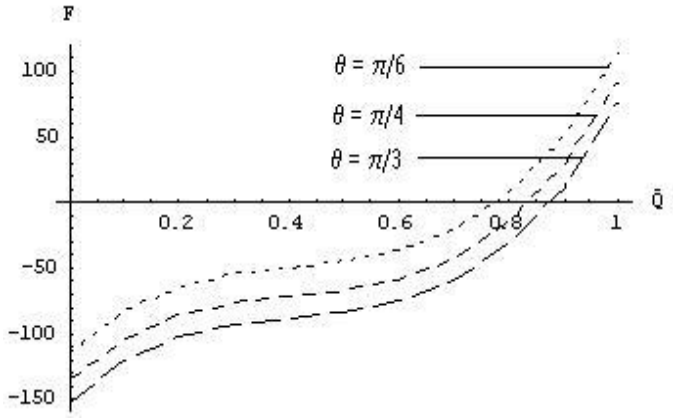

Figure 15. *n=3; =0.3; Da =0.3; =0.3; =0.1; =0.1.* Illustration of frictional force with the volume flow rate for various values of inclination of the channel in a divergent channel.

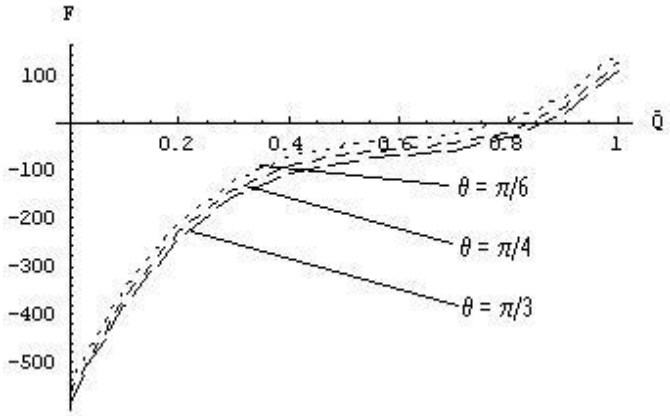

Figure 16. *n=3; =0.3; Da =0.3; =0.3; =0.1; =0.1.*Illustration of frictional force with the volume flow rate for various values of inclination of the channel in a convergent chann**el.**

4. Conclusion

The peristaltic flow of Herschel-Bulkley fluid is considered in a non-uniform inclined channel, in the wave frame of reference moving with the velocity of the wave. Low Reynolds number and long wavelength assumptions are applied to resolve the model. Solution is obtained for the pressure difference ΔP and the frictional force F against the time average volume flow rate $\bar{Q}$. Mathematica software is used to draw the various plots. The outcomes of the present investigation are:

- Increase in the porous thickening ϵ increases the pumping.
- As the yield stress τ enhances the pressure difference ΔP also enhances.
- Elevating the angle of intersection θ, we notice that the pressure difference ΔP also increases.
- For the Darcy number *Da*, the behavior is seen to reverse. When the Darcy number *Da* increases, the pressure difference ΔP is seen to decrease.
- Increase in the porous thickening ϵ decreases the frictional force F.
- As the yield stress τ enhances, the frictional force diminishes.
- Elevating the angle of inclination θ, the frictional force F decreases.
- With regard to the frictional force F, it is observed that frictional force increases with the Darcy number, and hence we observe reduced flow rate.

We thus can say that improving the values of these parameters of the Darcy number *Da*, porous thickening ϵ, and the yield stress τ, we can enhance the flow rate. The behavior mentioned above is the same for both the convergent and divergent channels for all the parameters under consideration. But, we see that the effect is more in a convergent channel when compared with a divergent channel for the porous thickening of the wall, yield stress, and the Darcy number. For the angle of inclination the effect is more in a divergent channel than in a convergent channel.

Finally for all factors we observe that the behavior of the frictional force is contrary to that of the pressure difference. This result agrees with the results of Vajravelu (2005), Sobh (2008).

Acknowledgment:

The authors are immensely grateful to the Editor and Reviewers for their insight and constructive suggestions that have enabled us to improve the quality of the manuscript.

REFERENCES

Abd ElHakeem, Abd ElNaby and ElMisery A.E.M. (2002). Effects of endoscope and generalized Newtonian fluid on peristaltic motion.Applied Mathematics and computation. Vol. 128(1), pp: 19-35.

Abd ElHakeem, Abd ElNaby and ElShamy, I. I. E. (2007). Slip effects on peristaltic transport of power-law fluid through an inclined tube. Appl. Math. Sciences. Vol. 1, pp: 2967-2980.

Akbar, N. S. and Adil Butt. (2015). Heat transfer analysis for the peristaltic flow of Herschel Bulkley fluid in a non-uniform inclined channel. Z. Naturforsch. Vol.70 (1), pp: 23–32.

Ali Abbas, M., Bai, Y. D., Bhatti, M. M. and Rashidi, M. M. (2016). Three dimensional peristaltic flow of hyperbolic tangent fluid in non-uniform channel having flexible walls, Alexandria Engineering Journal, Vol. 55(1), pp: 653–662.

Ali Abbas, M, Bai, Y. D., Rashidi, M. M. and Bhatti, M. M. (2015). Application of drug delivery in magneto hydrodynamics peristaltic flow of hyperbolic tangent fluid in non-uniform channel having flexible walls.Journal./doi/abs/10.1142/S0219519416500524.

Amit Medhavi (2008). Peristaltic Pumping of a Non-Newtonian Fluid. Appl. Appl. Math. Vol. 3(1), pp: 137–148.

Bhatti, M. M. and Ali Abbas, M. (2016). Simultaneous effects of slip and MHD on peristaltic blood flow of Jeffrey fluid model through a porous medium. Alexandria Engineering Journal.doi 10.1016/j.aej.2016.03.002.

Brown, T. D. and Hung, T. K. (1977). Computational and experimental investigations of two-dimensional nonlinear peristaltic flows. J. Fluid Mechanics, Vol. 83(2), pp: 249–272.

Ebaid. A. (2008). Effects of magnetic field and wall slip condition on the peristaltic transport of a Newtonian fluid in an asymmetric channel. Phys. letters A. Vol. 372(24), pp: 4493–4499.

Ellahi, R., Bhatti, M. M. and Arshad. Kiaz. (2014). Effects of magneto hydrodynamics on peristaltic flow of Jeffery fluid in a rectangular duct through a porous media.Journal of porous media. Vol. 17, pp: 143–157.

Ellahi, R., Bhatti, M. M. and Vafai, K. (2014).Effects of heat and mass transfer in a non-uniform rectangular. Journal of heat and mass transfer. Vol.71, pp: 706–709. dio:10.1016/j.ijheatmasstransfer.2013.12.038.

Elshehawey, E. F., Eldabe, N. T., Elghazy, E. M. and Ebaid, A. (2006).Peristaltic transport in an asymmetric channel through a porous medium. Applied Mathematics and Computation. Vol. 182(1), pp: 140–150.

Hummady, L. Z. and Abdulhadi, A. M. (2014). Effect of heat transfer on the peristaltic transport of MHD with couple-stress fluid through a porous medium with slip effect. Mathematical Theory and Modeling. IISTE, Vol.4 (7), pp: 1–18.

Hung, T. K. and Brown, T. D. (1976). Solid-particle motion in two-dimensional peristaltic flows. J. Fluid Mechanics. Vol. 73(1), pp: 77–96.

Krishna Kumari, S. V. H. N. P., Saroj, D. Vernekar. and Ravi Kumar, Y. V. K. (2013). Peristaltic motion of a Micropolar fluid under the effect of a magnetic field in an inclined channel. The International Journal of Engineering and Science (IJES) Vol. 2 (12); pp: 31–40.

Majhi, S. N. and Nair, V. R. (1996). Pulsatile flow of third grade fluids under body acceleration- modeling blood flow, Int. J. Engg. Sci. Vol. 32(5), pp: 839–846.

Mekheimer, K. S. (2002). Peristaltic transport of a couple stress fluid in uniform and non-uniform channels. Biorheology.Vol. 39(6), pp: 755–765.

Mishra, J. C. and Ghosh, S. K. (1997). A mathematical model for the study of blood flow through a channel with permeable walls. Acta mechanica.Vol.122, pp: 137–153.

Misra and Rao, A. R. (2003). Peristaltic transport of a Newtonian fluid in an asymmetric channel. Z Angew, Math. Phys. Vol. 54, pp: 530–550.

Nagachandrakala, G., Leelarathnam, A. and Sreenadh, S. (2013). Influence of slip conditions on MHD peristaltic flow of a hyperbolic tangent fluid in a non-uniform porous channel with wall properties. International Journal of Engineering Science & Technology, Vol. 5 (5), pp: 951–963.

Raju, K. K. and Devanathan, R. (1972). Peristaltic motion of a non-Newtonian fluid.Rheol.Acta.Vol.11, pp: 170–179.

Ramana, Kumari and Radhakrishnamacharya (2011). Effect of slip on peristaltic transport in an inclined channel with wall effects. Int. J. of Appl. Math and Mech.Vol.7(1), pp:1–14.

Ramesh, K. and Devakar, M. (2015). Peristaltic transport of MHD Williamson fluid in an inclined asymmetric channel through porous medium with heat transfer. J.Cent. South univ. Vol. 22, pp: 3189–3201.

Rathod, V. P. and Sridhar, N. G. (2015). Peristaltic Flow of A Couple Stress Fluids in an Inclined Channel. International Journal of Allied Practice, Research and Review. Vol.II, (VII), pp: 27–38.

Riahi, D. N. and Ranadhir Roy. (2011). Mathematical Modeling of Peristaltic Flow of Chyme in Small Intestine.Appl. Appl. Math. Vol. 6(2), pp: 428 – 444.

Sankad, G. C., Nagathan, P. S., Asha Patil and Dhange, M. Y. (2014). Peristaltic Transport of a Herschel-Bulkley Fluid in a Non-Uniform Channel with Wall Effects. International Journal of Engineering Science and Innovative Technology (IJESIT) Vol. 3(3), pp: 669–678.

Scheidegger, A. E. (1974). The Physics of Flow through Porous Media.3rd edition, University of Toronto press, Toronto, Canada.

Shapiro, A. H., Jaffrin, M. Y and Weinberg, S. L. (1969). Peristaltic pumping with long wavelengths at low Reynolds number, J. Fluid Mech. Vol.**37**, pp: 799-825.

Smita Dey and Anamol Kumar Lal. (2013). Study of Peristaltic Flow of Blood in Artery International Journal of Sciences: Basic and Applied Research (IJSBAR), Vol.12(1): pp 220-228.

Sobh, A. M. (2008). Interactions of couple stresses and slip flow on peristaltic transport in uniform and non-uniform channels. Turkish Journal of Engineering Environmental Sciences. Vol. 32, pp: 117-123.

Tang, H. T. and Fung, Y. C. (1975). Fluid movement with permeable walls covered by porous media. A model of lung alveolar sheet. J. Appl. Mech. Vol. 97, pp: 45-50.

Vajravelu, K., Sreenadh, S. and Ramesh Babu, V. (2005). Peristaltic pumping of a Herschel Bulkley fluid in a channel. Applied Mathematics and Computation.Vol.169, pp: 726-735.

Appendix

From the governing equation

$$\frac{\partial}{\partial y}(\tau_{yx}) = -\frac{\partial p}{\partial x} + \eta\, sin\theta, \tag{1.1}$$

where

$$\tau_{yx} = \left(-\frac{\partial u}{\partial y}\right)^n + \tau_0\,, \tag{1.2}$$

and

$$\tau_{yx} = 0 \;\; at \;\; y = 0\,, \tag{1.3}$$

Solving Equations (1.1) and (1.2) along with the boundary condition (1.3), we get

$$\frac{\partial u}{\partial y} = -(Py - \tau_0)^{\frac{1}{n}}\,. \tag{1.4}$$

Introducing $u = \frac{\partial \psi}{\partial y}$, we obtain

$$\psi = \frac{(Py-\tau_0)^{\frac{1}{n}+2}}{(\frac{1}{n}+1)(\frac{1}{n}+2)P^2} + Ay + B, \tag{1.5}$$

where *A* and *B* are constants determined by using the boundary conditions (1.6) and (1.7)

$$\psi = 0 \;\; at \;\; y = 0\,, \tag{1.6}$$

$$u = -\frac{\sqrt{Da}}{\alpha}\frac{\partial u}{\partial y} - 1 \;\; at \;\; y = h(x) - \epsilon. \tag{1.7}$$

Thus, we obtain the velocity as in Equation (8)

$$u = P^m\left[\frac{1}{m+1}\{(h-\epsilon-y_o)^{m+1} - (y-y_o)^{m+1}\} + \frac{\sqrt{Da}}{\alpha}(h-\epsilon-y_o)^m\right] - 1\,.$$